Supplementary information

Novel Metal enhanced dual-mode fluorometric and SERS aptasensor implicating heterostructure nanoassembly for ultrasensitive T-2 Toxin detection

Imran Mahmood Khan[a,b], Sobia Niazi[a,b*], Imran Pasha[c], Muhammad Kashif Iqbal Khan[c], Lin Yue [a,b], Ye Hua[d], Ali Mohsin[e], Muhammad Shoaib[a,b], Yin Zhang[g], Zhouping Wang[a,b,f*]

[a]State Key Laboratory of Food Science and Technology, Jiangnan University, Wuxi, China.

[b]School of Food Science and Technology, Jiangnan University, Wuxi, China.

[c]NIFSAT, University of Agriculture, Faisalabad, Pakistan.

[d]School of Grain Science and Technology, Jiangsu University of Science and Technology, Zhenjiang,212004, China.

[e]State Key Laboratory of Bioreactor Engineering, East China University of Science and Technology, Shanghai 200237, PR China

[f]Key Laboratory of Meat Processing of Sichuan, Chengdu University, Chengdu, 610106, China.

Corresponding authors: Zhouping Wang and Sobia Niazi

AUTHOR EMAIL(S): wangzp@jiangnan.edu.cn;sobianiazi@jiangnan.edu.cn

Postal address: Jiangnan University, No. 1800 Lihu Avenue, Wuxi, Jiangsu, 214122, P.R.C

Apparatus and characterization

Fluorescent spectra were measured by a Hitachi F-7000 fluorescence spectrophotometer (Hitachi Co., Japan). UV–vis spectra were recorded on a UV-1800 spectrophotometer (Shimadzu Co., Japan). JEM-2100HR transmission electron microscope operating at 200 kV acceleration voltage (TEM, JEOL Ltd., Japan) was used to characterize the size and morphology of nanostructures. TEM samples were prepared by pipetting five microliters of the solution onto carbon grids coated with an ultrathin carbon film. X-ray powder diffraction (XRD) patterns were obtained by a D8 Advance (Bruker AXS Ltd., Germany) with Cu-Kαradiation (λ=0.1540 nm). Raman Microscope Imaging Spectrometer was used to measure the SERS spectra with a 633 nm laser excitation, the 10× objective lens was used to focus the laser, and the Raman spectra were acquired from 400 to 1800 cm−1 with an integration time of 10 s.

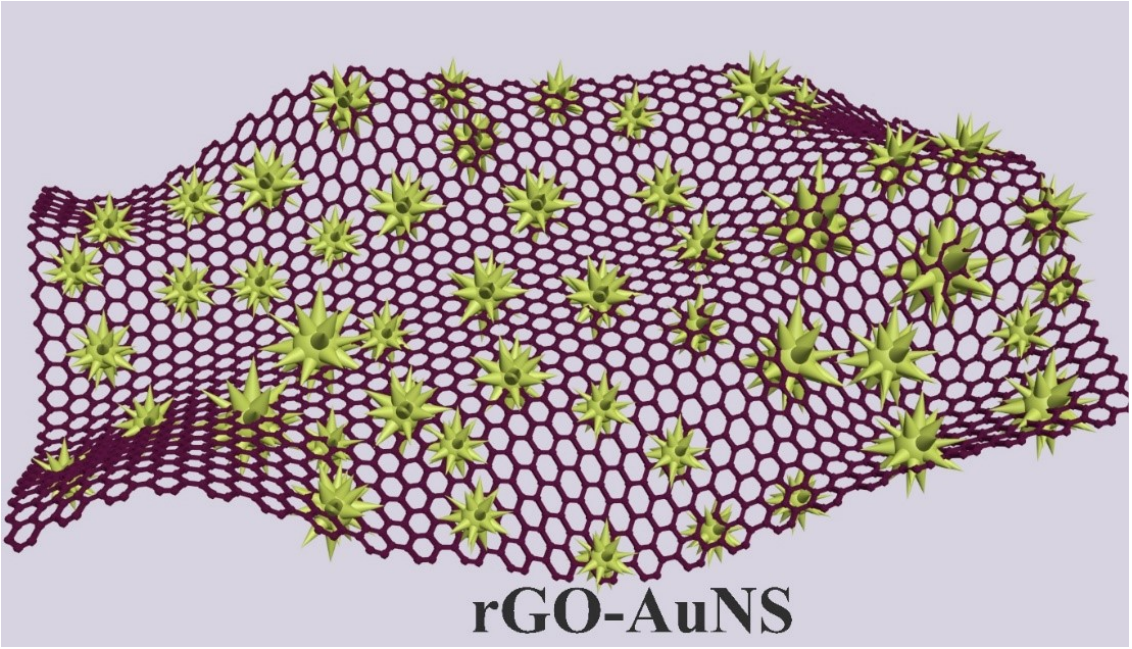

Fig. S1. rGO-AuNS nanocomplex

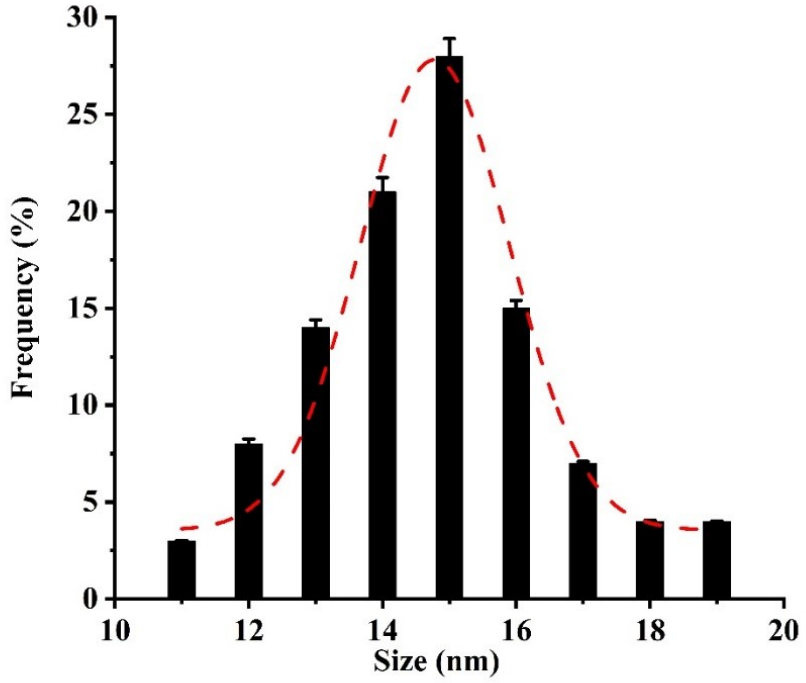

Fig. S2. AuNPs with an average size of 14.78 nm. (Error bars represent the mean of three replicate)

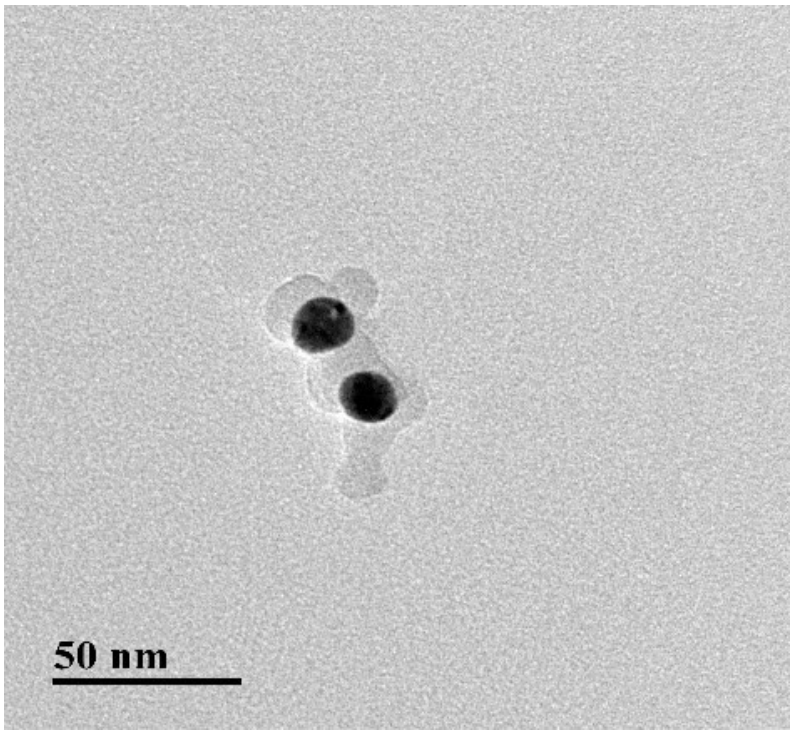

Fig.S3. AuNPs with first silica layer at 50 nm dimension.

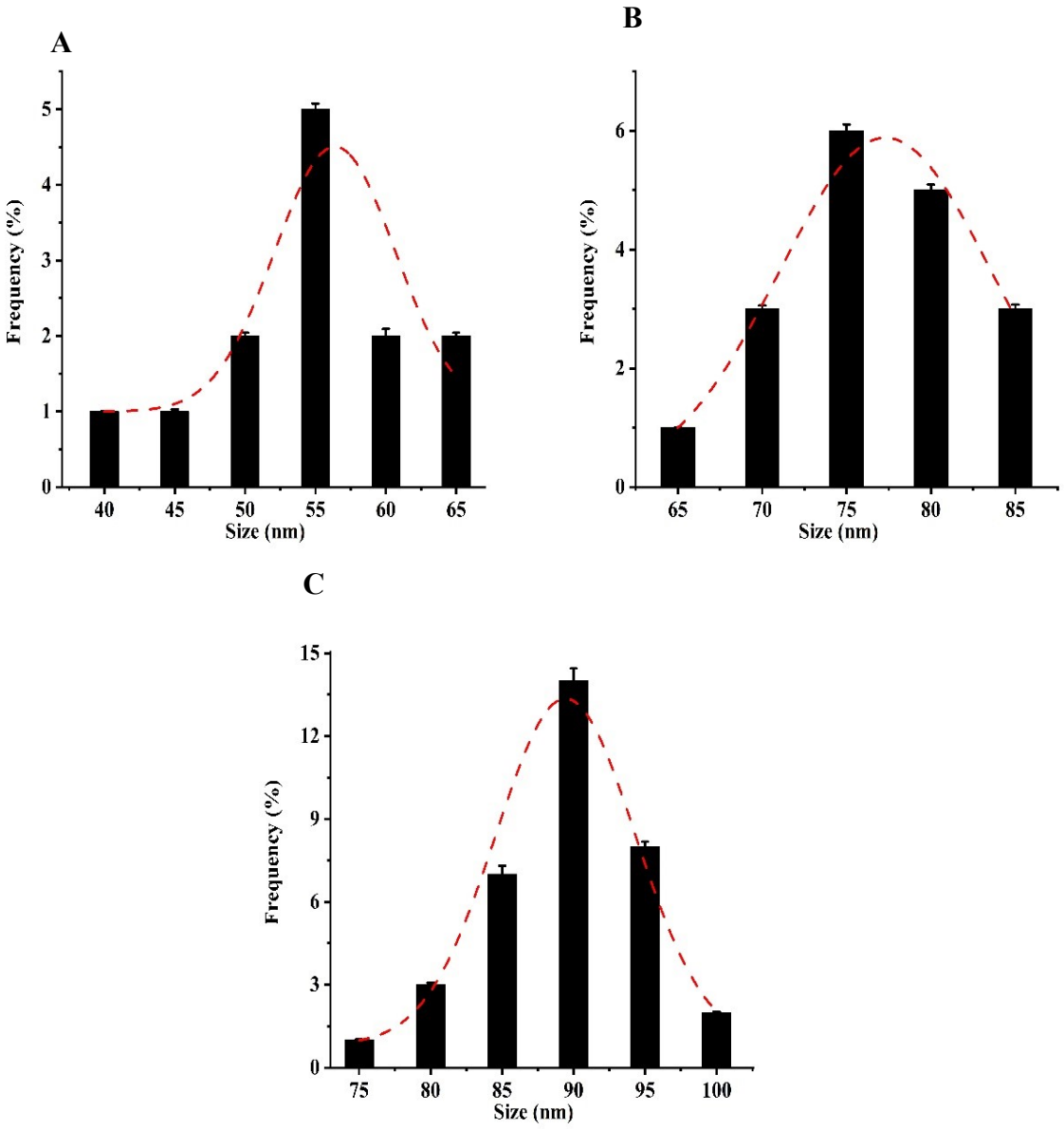

Fig. S4. (A) First RITC and silica stabilization. (B) Second stabilization of RITC and silica. (C) MPTS stabilization for thiol functionalization. (Error bars represent the mean of three replicate)

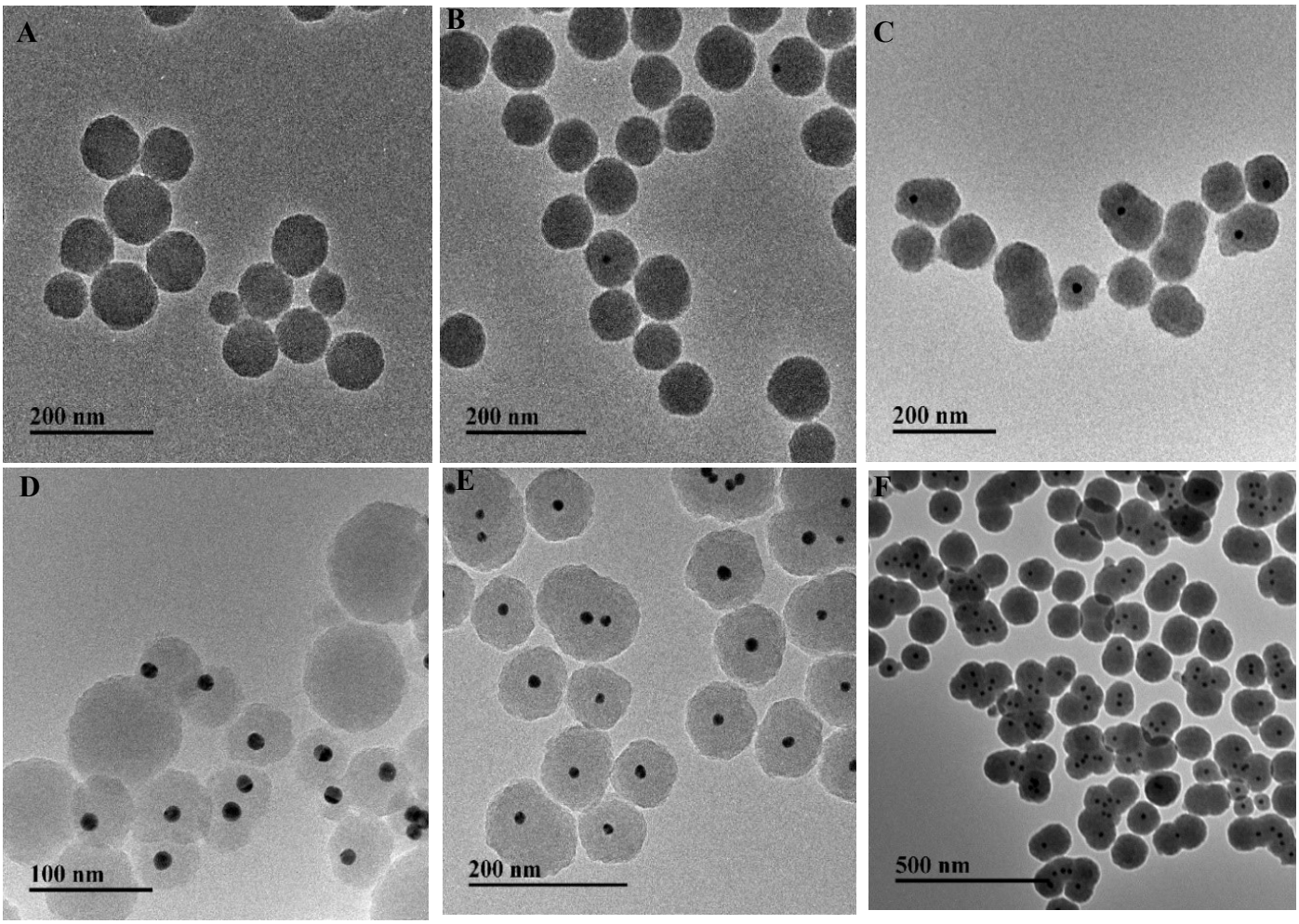

Fig. S5. Influence of different concentrations of AuNPs@PVP as core material on the RITC SiO_2. RITC SiO_2 with (A) 0 μL, (B) 3 μL, (C) 5 μL, (D) 10 μL, (E)15 μL, and (F) 20 μL.

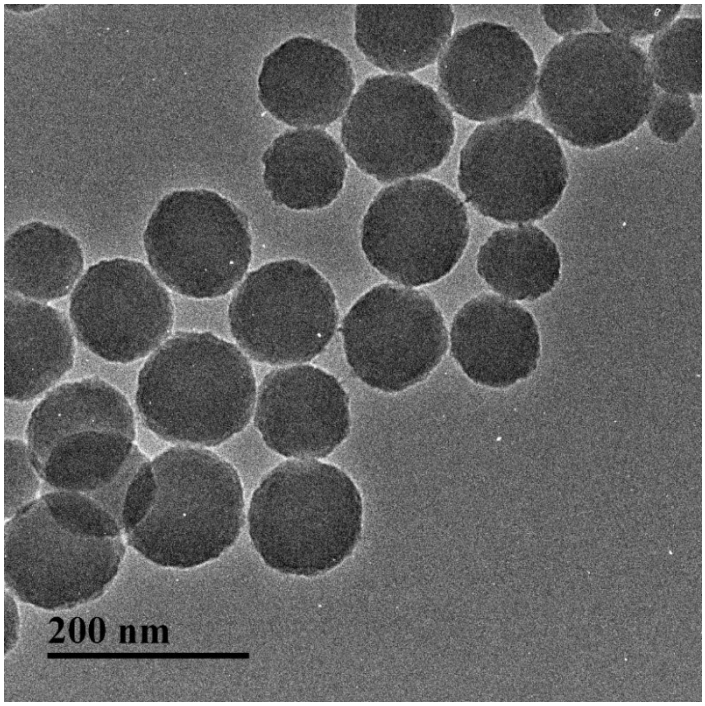

Fig. S6. TEM images of RITC SiO_2 NPs

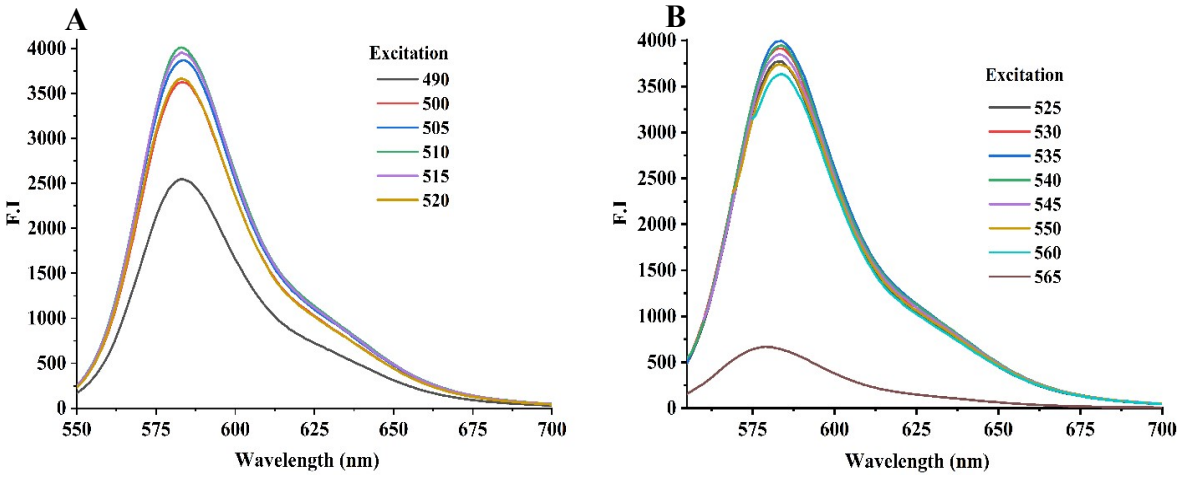

Fig. S7. The different excitation resulted in different intensities of emission. **(A)** The excitation wavelength from 490 to 520 nm. **(B)** The excitation wavelength from 520 to 565 nm.

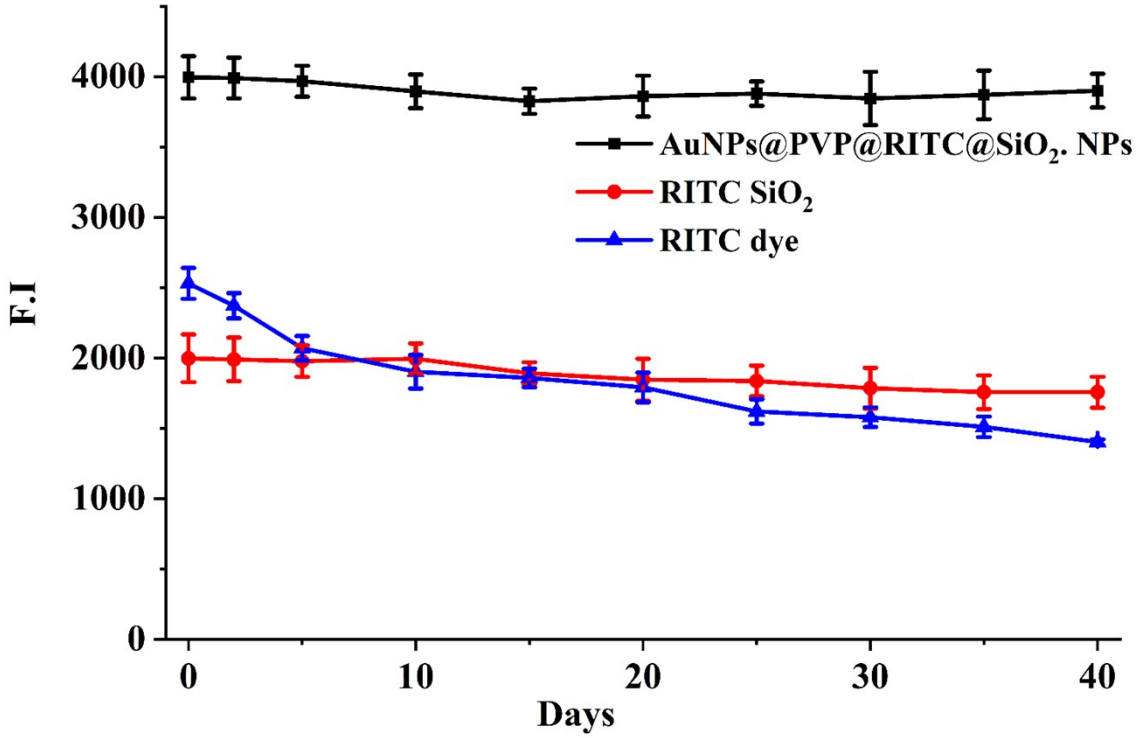

Fig. S8. The effect of room storage on the photostability of AuNPs@PVP@RITC@SiO_2. NPs, RITC-SiO_2, and RITC dye regarding F.I during the 40 days. (Error bars represent the mean of three replicate)

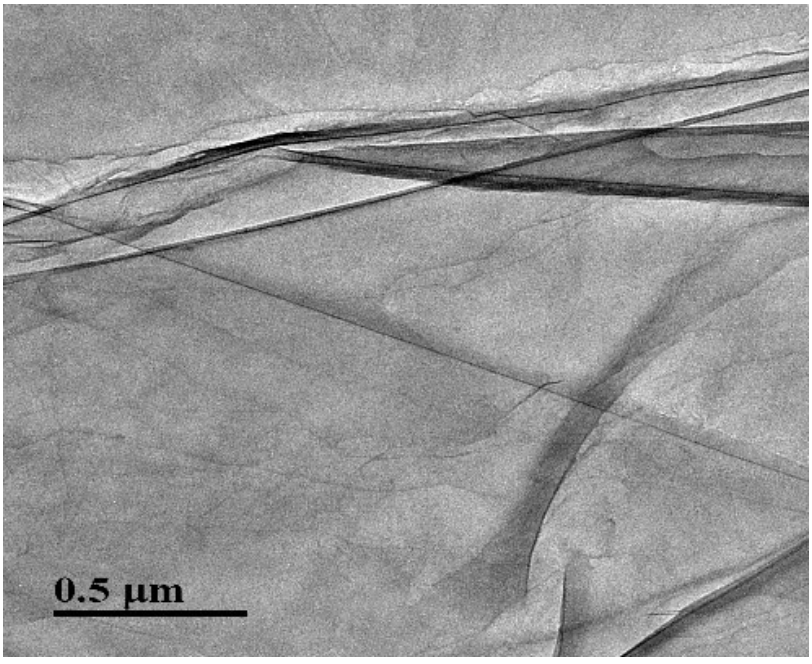

Fig.S9. Tem image of rGO at 500 nm dimension

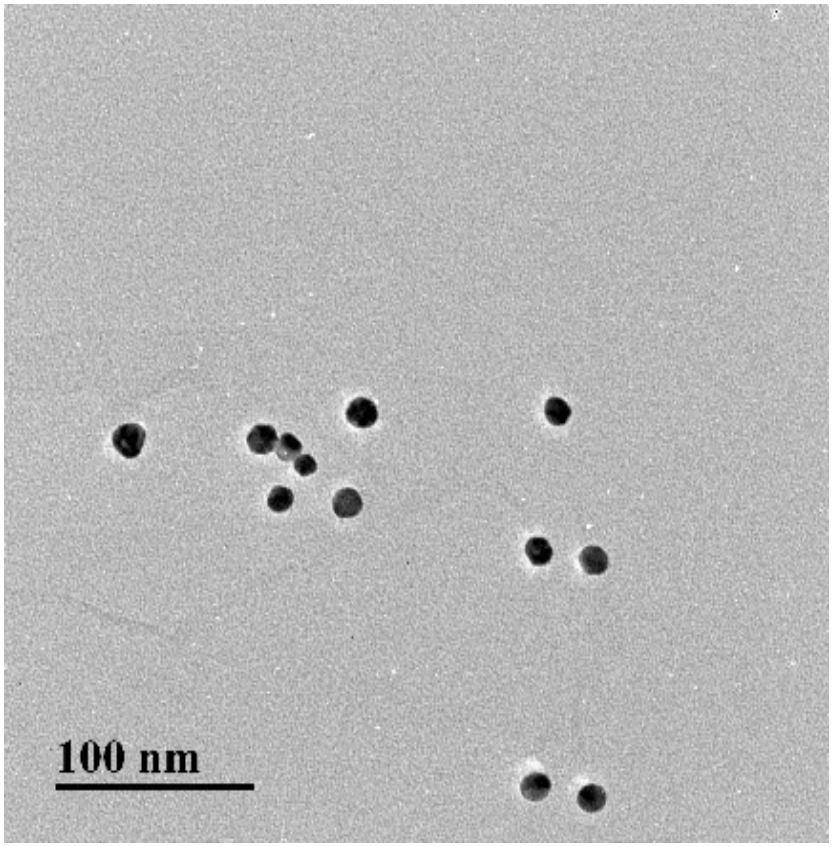

Fig. S10. Tem image of AuNPs anchored on the surface of rGO as seed solution (rGO-AuNPs) at 100 nm scale bar.

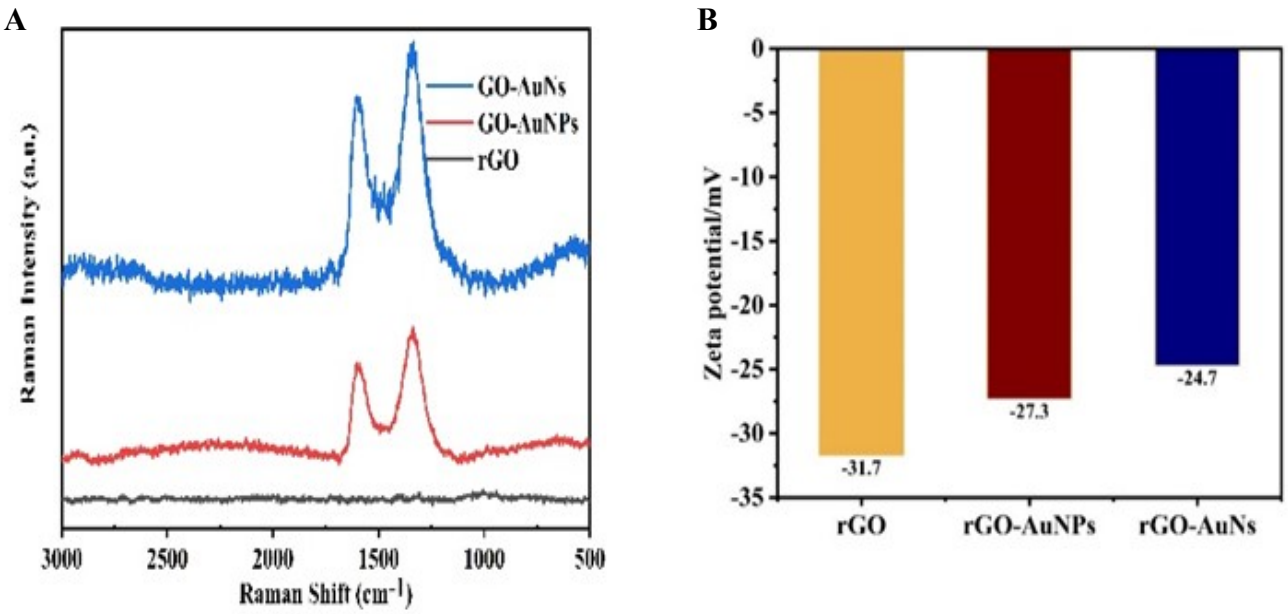

Fig.S11. (A) Raman spectra of rGO, rGO-AuNPs, and rGO-AuNS. (B) The zeta potential of rGO, rGO-AuNPs, and rGO-AuNS.

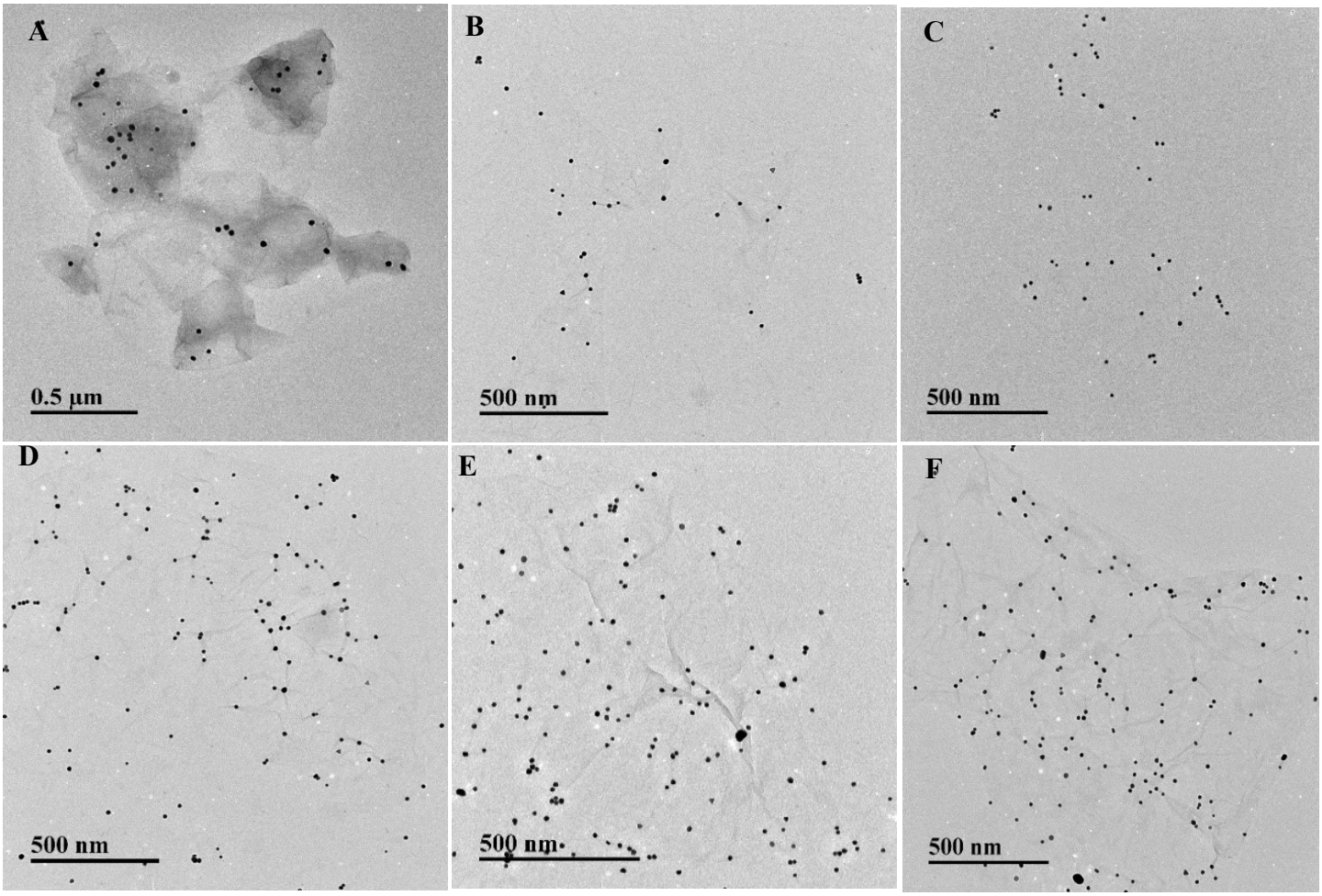

Fig. S12. The effect of different concentrations of Au salt (158.3 mM) on the rGO. (**A**) 40. (**B**) 50. (**C**) 60. (**D**)70. (**E**) 80. (**F**) 90 µL.

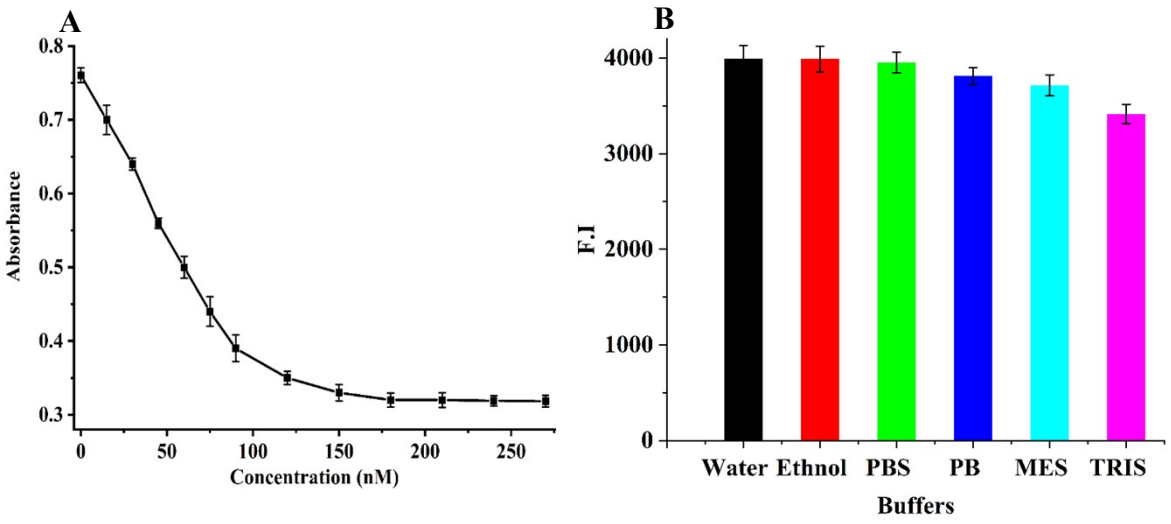

Fig. S13. (A) Incubation of different concentrations of T-2 aptamer (0-270 nM) with AuNPs@PVP@RITC@SiO_2. NPs. (B) The effect of different mediums on the photostability of AuNPs@PVP@RITC@SiO_2. NPs.

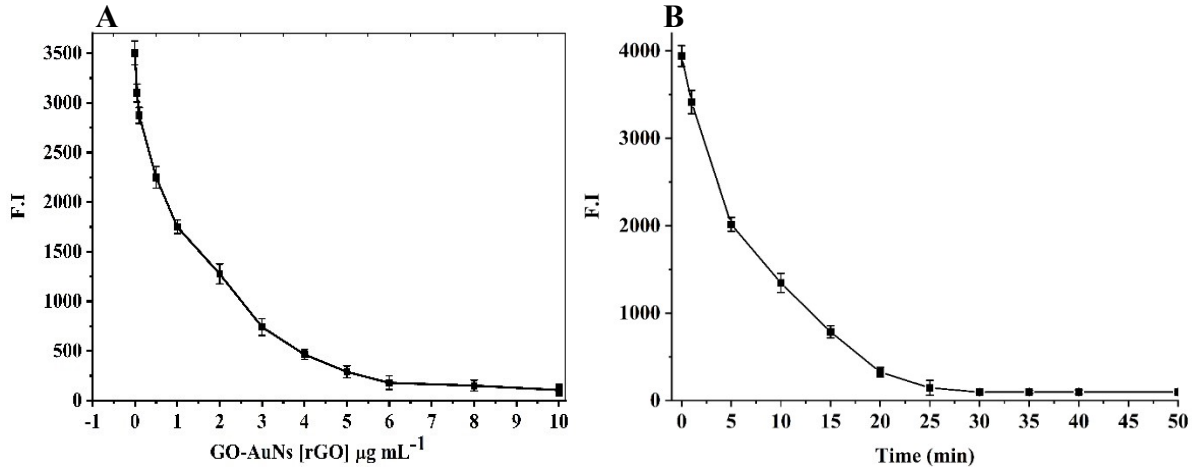

Fig. S14. (A)The effect of different concertation of GO-AuNS composite (0-10 µgmL^{-1}) to quench the F.I of Apt-AuNPs@PVP@RITC@SiO_2. NPs. (B) The effect of incubation time to quench the F.I of Apt-AuNPs@PVP@RITC@SiO_2. NPs.

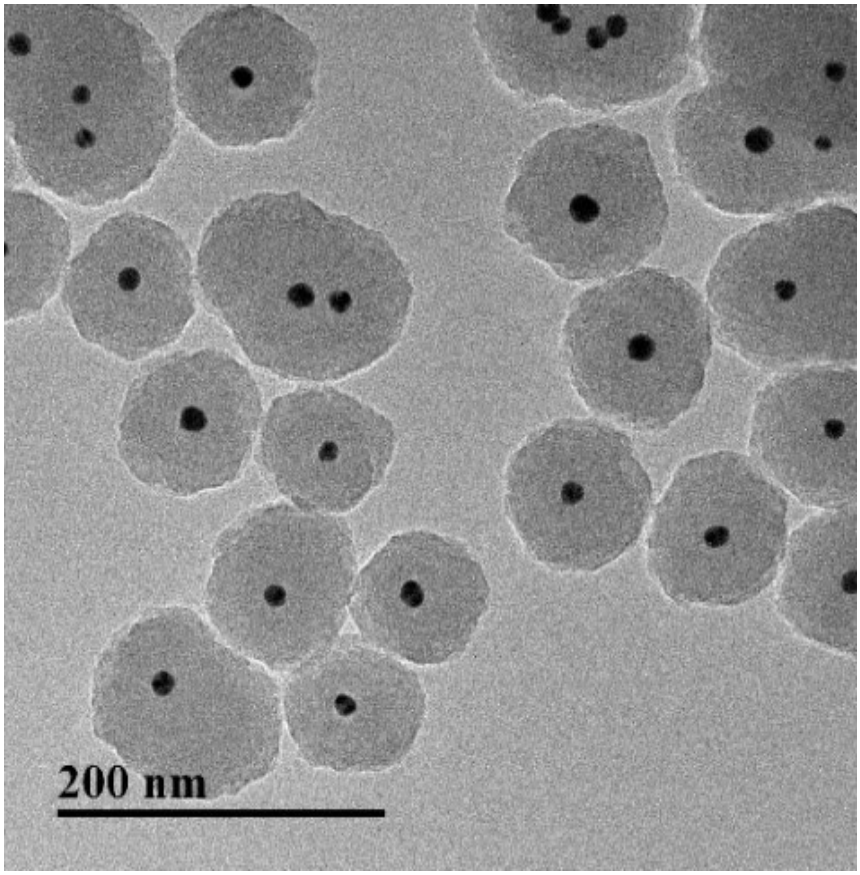

Fig.S15. Apt- AuNPs@PVP@RITC@SiO_2. NPs.

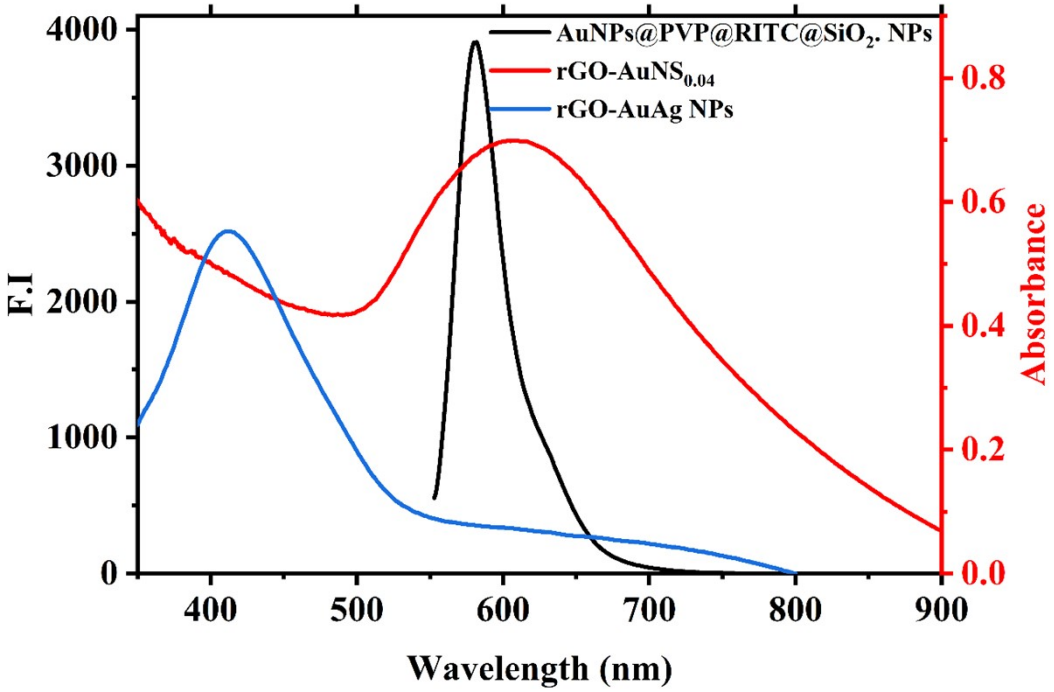

Fig. S16. The depiction of Spectral overlap between the F.I of Apt-AuNPs@PVP@RITC@SiO_2. NPs. and absorption spectra of rGO-$AuNS_{0.04}$ and rGO-AuAg NPs.

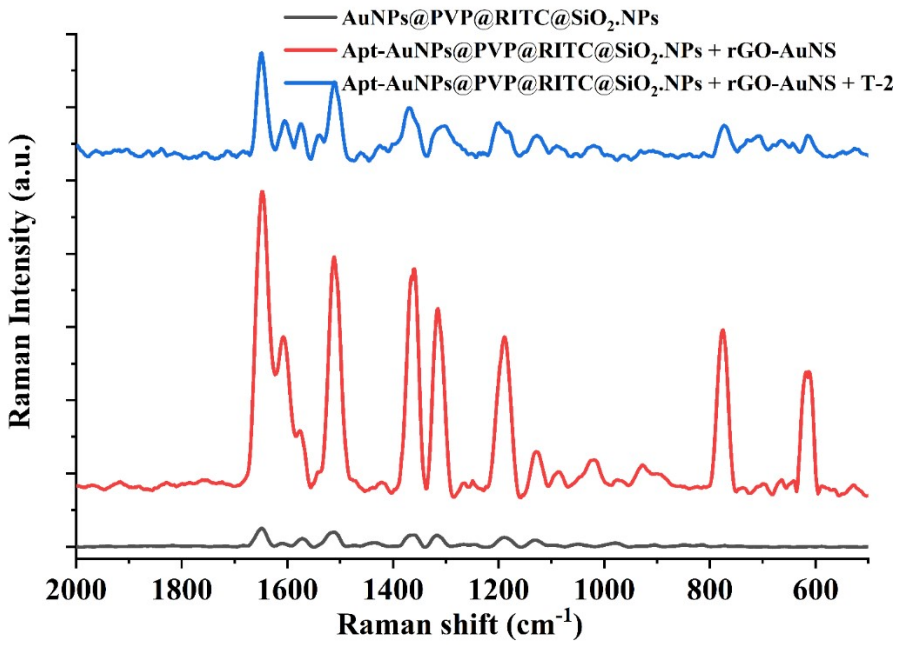

Fig. S17. SERS response of Apt-AuNPs@PVP@RITC@SiO_2. NPs under various analysis conditions.

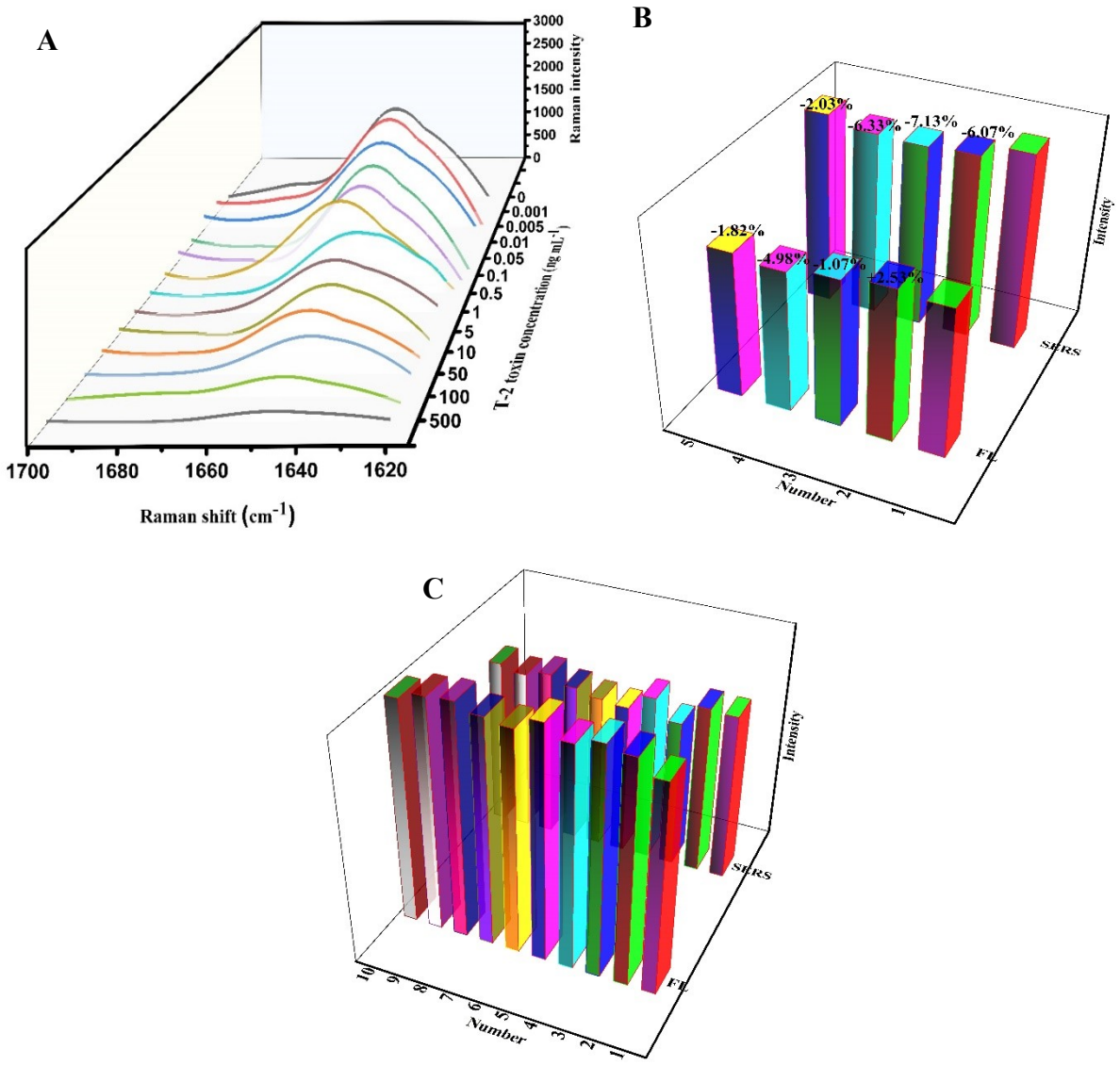

Fig. S18. (A). The enlarged view about f the intensity of the 1648 cm^{-1} peak against the logarithm of the T-2 toxin concentration. **(B)** The reproducibility of the designed dual-mode sensor. **(C)** The stability of the designed dual-mode sensor.

Table. S1. Comparison between developed method and different analytical methods for T-2 toxin

Method	Commodity	Working range	LOD	References
FL aptasensor	Milk	0.5–100 ng mL^{-1}	0.239 ng mL^{-1}	[1]
FL aptasensor	Wheat	0.005-500 ng mL^{-1}	0.93 pg mL^{-1}	[2]
Electrochemical sensor	Soybeans	1.12 nM -2.12 μM	0.33 nM	[3]
Target-responsive DNA hydrogel	Corn	0.01–1000 ng mL^{-1}	0.87 pg mL^{-1}	[4]
Time-resolved fluorescence immunochromatography (TRFIA)	Corn	0.0625–50 ng mL^{-1}	0.052 ng mL^{-1}	[5]
Lateral flow -TRFIA	Maize	0.125–200 ng g^{-1}	0.17 ng g^{-1}	[6]
Dual mode FL-SERS aptasensor	Maize and Wheat	(0.001-500 ng mL^{-1})	0.85 pg mL^{-1} for FL and 0.12 pg mL^{-1} for SERS	This study

References

1. X. Zhao, Y. Wang, J. Li, B. Huo, Y. Qin, J. Zhang, M. Chen, Y. Peng, J. Bai, S. Li and Z. Gao, *Spectrochim. Acta, Part A*, 2021, **259**, 119893.
2. I. M. Khan, S. Zhao, S. Niazi, A. Mohsin, M. Shoaib, N. Duan, S. Wu and Z. Wang, *Sens. Actuators, B*, 2018, **277**, 328-335.
3. X. Gao, W. Cao, M. Chen, H. Xiong, X. Zhang and S. Wang, *Electroanalysis*, 2014, **26**, 2739-2746.
4. Y. Sun, S. Li, R. Chen, P. Wu and J. Liang, *Sens. Actuators, B*, 2020, **311**, 127912.
5. L. Wei, J. Zhang, C. Zha, Q. Yang, F. Li, X. Sun, Y. Guo and Z. Liu, *Eur. Food Res. Technol.*, 2022, **248**, 457-466.
6. Z. Zhang, D. Wang, J. Li, Q. Zhang and P. Li, *Anal. Methods*, 2015, **7**, 2822-2829.